NANO · MICRO small
www.small-journal.com

Amorphous Mn_3O_4 Nanocages with High-Efficiency Charge Transfer for Enhancing Electro-Optic Properties of Liquid Crystals

Guanshui Ma, Binbin Jia, Dongyu Zhao, Zhao Yang, Jian Yu, Juzhe Liu, and Lin Guo**

Improving electro-optic properties is essential for fabricating high-quality liquid crystal displays. Herein, by doping amorphous Mn_3O_4 octahedral nanocages (a-Mn_3O_4 ONCs) into a nematic liquid crystal (NLC) matrix E7, outstanding electro-optic properties of the blend are successfully obtained. At a doping concentration of 0.03 wt%, the maximum decreases of threshold voltage (V_{th}) and saturation voltage (V_{sat}) are 34% and 31%, respectively, and the increase of contrast (C_{on}) is 160%. This remarkable electro-optic activity can be attributed to high-efficiency charge transfer within the a-Mn_3O_4 ONCs NLC system, caused by metastable electronic states of a-Mn_3O_4 ONCs. To the best of our knowledge, such remarkable decreased electro-optic activity is observed for the first time from doping amorphous semiconductors, which could provide a new pathway to develop excellent energy-saving amorphous materials and improve their potential applications in electro-optical devices.

Liquid crystal display (LCD) devices have been indispensable elements of life in the past decade with the progress in liquid crystals (LCs), due to the ubiquity of their applications from wristwatch to personal computer displays.[1–8] Notably, a critical limitation in LCD devices is the electric double layer that engendered by the adsorbed ions. The electric double layer would diminish the effect of applied field and subjoin the driving voltages of liquid crystals, leading to the depletion of energy.[9,10] To combat this problem, dispersion of nanoparticles (NPs) as active-matrix component optimizing the electro-optic (E-O) properties of LCs is regarded as a quick and economical method.[11–21] For incorporation of NPs in LC matrix, the proper selection of crystallographic phase, capping agent, shape, and size of the NPs is critical for the performance of the blend.[22,23] For example, Kinkead et al.[24] synthesized hexadecylamine-capped CdSe and thioglycolic acid-capped CdTe semiconductor quantum dots (QDs) varying in size from 2.5 to 5.2 nm, and doped them into nematic liquid crystals (NLCs). They found that all QDs were effective in reducing the threshold voltage (V_{th}), and the two most promising QDs $CdSe_{480}$ and $CdSe_{590}$ QDs in NLC showed the lowest drop of V_{th} values at 2 and 5 wt%. Acharya and co-workers[25] incorporated ultranarrow ZnS nanorods in the NLCs to lowing driving voltages. Previously unachieved and robust electro-optic properties were obtained with the V_{th} of blends substantially reduced by up to 10%. Another examples of hybrid NPs are the suspensions of ferroelectric nanoparticles in liquid crystals[26] Buchnev and co-workers prepared ferroelectric particles of $Sn_2P_2S_6$ and $BaTiO_3$ nanoparticles with sizes in 45 and 20 nm respectively, and doped them into liquid crystals. The threshold voltage reduction of more than 50% was demonstrated,[27] as well as the improvement in the response time.[28]

One NPs candidate for this doping method is amorphous semiconductor nanomaterials. Since their disordered long-range atomic arrangement and accommodating inherent abundant defects endow amorphous nanomaterials with dangling bonds and band tails, which could lead the energy to a metastable state and thus facilitate the surface electron escape and transfer.[29–33] Combining these advantages, enhancement of interaction between amorphous semiconductor and the NLCs molecule could be achieved when doping amorphous semiconductor into NLCs. However, doping amorphous semiconductor materials with liquid crystal for improving the electro-optical performance has rarely been reported.

Motivated by these tantalizing prospects, here we report a novel semiconductor nanomaterial for competitive electro-optic technology, that is, amorphous Mn_3O_4 octahedral nanocages (a-Mn_3O_4 ONCs). We show that with a trace amount concentration dispersion of a-Mn_3O_4 ONCs in NLCs matrix E7, a markedly decrease of V_{th} and saturation voltage (V_{sat}), a higher contrast (C_{on}), and a shorter response time (T_{total}) are achieved (the detail meanings of V_{th}, V_{sat}, C_{on}, and T_{total} are in experimental section.). To the best of our knowledge, this is the first report of enhancing E-O properties by doping inorganic amorphous semiconductor NPs. Our general approach of doping a-Mn_3O_4 ONCs into E7 could be explored to design composites consisting of other inorganic amorphous semiconductor nanomaterials and different types of LCs, and could improve their potential applications in electro-optical technologies, which could be used in portable devices.

A Mn_3O_4 nanomaterial was selected as an ideal candidate nanomaterial dopant into LCs for improving the E-O

G. Ma, B. Jia, Prof. D. Zhao, Z. Yang, J. Yu, J. Liu, Prof. L. Guo
Beijing Advanced Innovation Center for Biomedical Engineering
Key Laboratory of Bio-Inspired Smart Interfacial Science and Technology
Ministry of Education
School of Chemistry
Beihang University
Beijing 100191, P. R. China
E-mail: zhaodongyu@buaa.edu.cn; guolin@buaa.edu.cn

The ORCID identification number(s) for the author(s) of this article can be found under https://doi.org/10.1002/smll.201805475.

DOI: 10.1002/smll.201805475

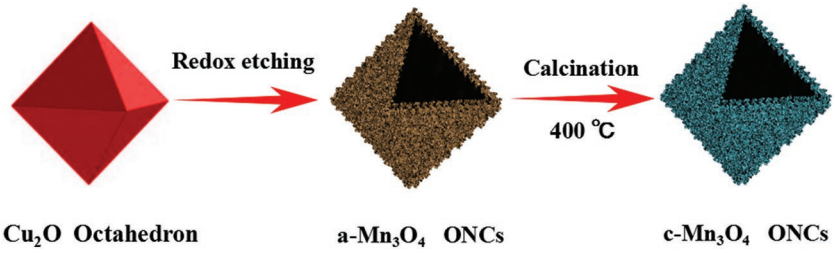

Scheme 1. A schematic of fabrication process for hollow amorphous and crystalline Mn_3O_4 octahedral nanocages structures by acid-engaged coordinating etching of Cu_2O.

technology, since the outer electrons of Mn^{2+} and Mn^{3+} were arranged as d^{5+} and d^{4+}, there were more single electron in the two ionic structures,[34,35] which produced the charge transfer on the surface much easier among reported semiconductor nanomaterials.[36,37] The synthesis procedures of hollow amorphous and crystalline Mn_3O_4 octahedral nanocages (c-Mn_3O_4 ONCs) structures were shown in **Scheme 1**. The details were given in the experimental section. First, we used an improved method to synthesize highly uniform Cu_2O octahedrons with our previous report method[38] (Figure S1a, Supporting Information). Subsequently, the highly uniform Cu_2O octahedrons were used as templates to synthesize the hollow a-Mn_3O_4 ONCs structures (Figure S1b, Supporting Information). Finally, with the help of thermogravimetric differential scanning calorimetry (TG-DSC) analysis (Figure S2, Supporting Information), the well-crystallized c-Mn_3O_4 ONCs (Figure S1c, Supporting Information) were obtained through a calcination on as-prepared a-Mn_3O_4 ONCs at 400 °C under Ar atmosphere. Interestingly, a typical broken composite nanocage supported that the Mn_3O_4 ONCs were hollow structures (Figure S1c, Supporting Information). Additionally, the as-prepared Mn_3O_4 ONCs exhibited high size uniformity and good shape regularity. The sizes of Mn_3O_4 ONCs were ≈550 nm according to statistical analysis from SEM images.

The transmission electron microscopy (TEM) images clearly showed a 3D octahedral structure constructed by 2D nanosheets (**Figure 1**a,b). The thickness of the nanocages was ≈50 nm, which was characterized by TEM (Figure S3, Supporting Information). The hollow feature was also verified by a color contrast between the pale center and dark edge. Both of the as-prepared hollow samples possess sharp edges and corners, which could be attributed to the successful shape duplication of the Cu_2O templates. Meanwhile, the atomic ration of Mn and O was about 3:4, which was confirmed by the EDS analysis (Figure S1d, Supporting Information), so we concluded that the prepared sample were a-Mn_3O_4 and c-Mn_3O_4 ONCs. In addition, the results of bright-field scanning TEM (BF-STEM) and EDX mapping analysis showed that Mn and O components distribute uniformly in the Mn_3O_4 ONCs (Figure S4, Supporting Information). The selected area electron diffraction (SAED) image of a-Mn_3O_4 ONCs in Figure 1c demonstrates the absence of a crystalline phase. In contrast, c-Mn_3O_4 ONCs had typical crystalline characteristics (Figure 1d). No lattice fringes were observed in high-resolution TEM (HRTEM) image in Figure 1e, suggesting the amorphous state of a-Mn_3O_4, which was consistent with its corresponding X-ray diffraction (XRD) pattern (Figure S5d, Supporting Information, no other peaks were seen, and this result further proved that the Mn_3O_4 ONCs were amorphous). For c-Mn_3O_4 ONCs, Figure 1f shows that the spacings of the adjacent lattice fringe were 0.308, 0.249, and 0.276 nm, which matched well with the lattice constants of (112), (211), and (103) planes in Figure 1d. In order to further study the composition and oxidation state of a-Mn_3O_4 ONCs, surface composition analysis with X-ray photoelectron spectroscopy (XPS) measurement was performed (Figure S5a–c, Supporting Information). The results confirmed well that the samples with multiple valences of Mn^{2+} and Mn^{3+} were successfully fabricated and the binding energy separation of Mn 3s peaks was ≈5.5 eV, which was consistent with that of Mn_3O_4 reported before.[34,35,39]

In addition, a suitable acid, phosphoric acid in this case, has been proven to play an important role on keeping the integrity of a-Mn_3O_4 nanocages. Hydrochloric acid as a stronger acid would lead to the collapse of nanocages due to the rapid reaction and produce debris formed by the small nanosheets (Figure S6a, Supporting Information), while a weaker acid, boric acid (Figure S6b, Supporting Information) would hardly etch the Cu_2O templates. With the adding of phosphoric acid, well-shaped a-Mn_3O_4 nanocages were successfully obtained without any dispersed Mn_3O_4 debris (Figure S6c, Supporting Information). In the first place, it was assumed that MnO_4^- ions would not basically react with Cu_2O in a mild environment and tended to adsorb on the surface of Cu_2O, with the addition of phosphoric acid, the oxidation of MnO_4^- was enhanced and the reaction with Cu_2O was accelerated. In this stage, as the reaction progresses, the Cu^{2+} ions gradually permeated out and the hollow a-Mn_3O_4 nanocages were successfully obtained. Furthermore, to demonstrate the effect of crystallinity on E-O performance of LCs, the amorphous-crystalline Mn_3O_4 ONCs (Figure S7, Supporting Information) were obtained through calcination on as-prepared c-Mn_3O_4 ONCs at 300 °C under Ar atmosphere. Through the HRTEM and SAED images clearly showed that Mn_3O_4 ONCs were crystallized but not completely.

Since the designed hollow structure of c-Mn_3O_4 ONCs provided us a promising platform to develop E-O technology, the E-O properties of a-Mn_3O_4-doped in E7 (the detail composition of E7 was shown in Figure S8, Supporting Information) were investigated. For an LC cell filled with pure E7, values of E-O parameters including V_{th}, V_{sat}, C_{on}, and T_{total} was 1.56, 2.24 V, 20 and 7.66 ms, respectively. As shown in **Figure 2**a, the curves for the voltage dependence of the transmittance (*V*–Tr) exhibit an increasing gradient with increasing a-Mn_3O_4 ONCs concentration. As the concentration of a-Mn_3O_4 ONCs increased from 0.01 to 0.03 wt%, V_{th} and V_{sat} gradually decreased (Table S1, Supporting Information). While when the concentration of a-Mn_3O_4 ONCs was greater than 0.03 wt%, V_{th} and V_{sat} started to slightly increase. At the concentration of 0.03 wt%, V_{th} and V_{sat} got the minimal and the maximum drop of V_{th} and V_{sat} reached 34% and 31%, respectively. This was a marked drop in V_{th} and V_{sat} value compared with other many microscale nanomaterial composites as reported in previous literatures (Table S2, Supporting Information). Simultaneously, *V*–Tr curves for LCs cells doped with c-Mn_3O_4 ONCs were detected for comparison

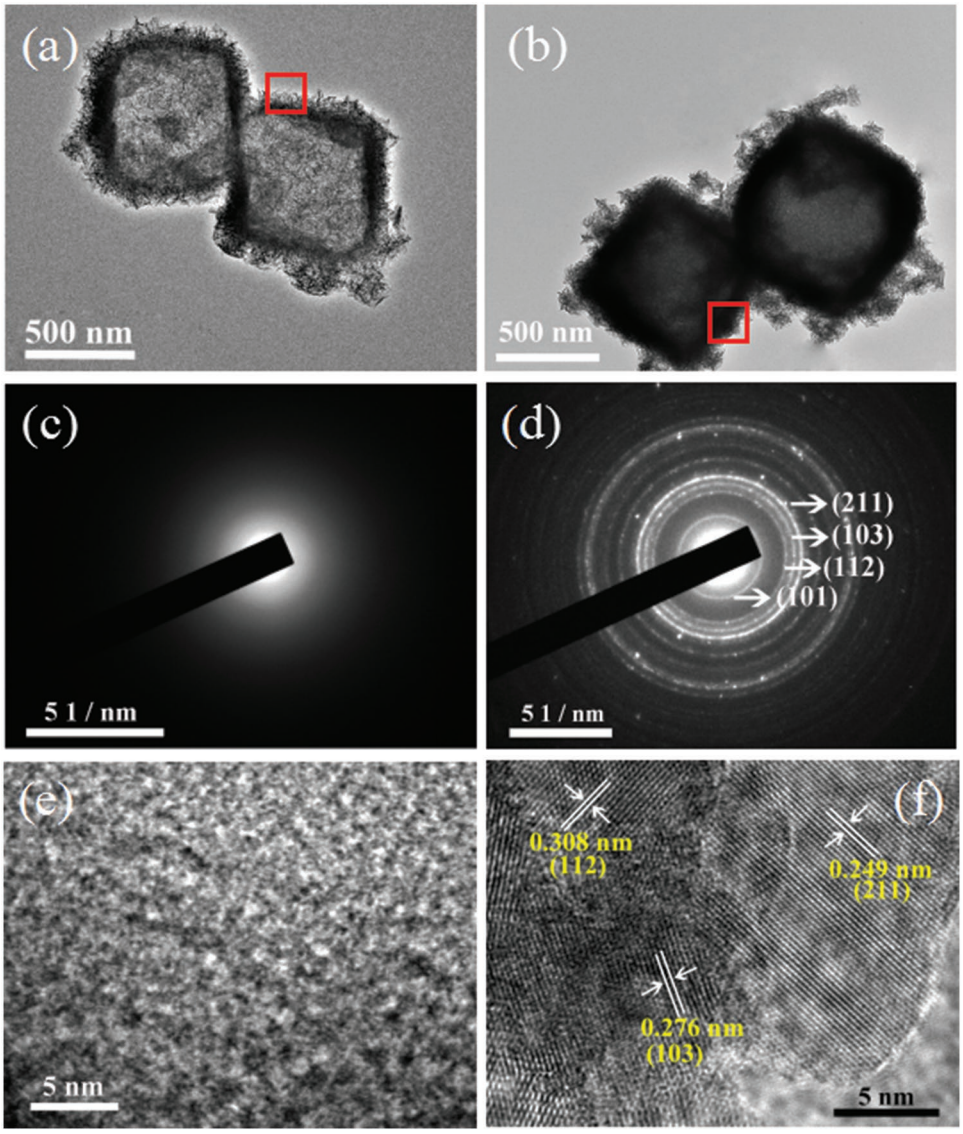

Figure 1. a,b) TEM images of a- and c-Mn_3O_4 ONCs. c,d) The SAED patterns of a- and c-Mn_3O_4 ONCs. e,f) The HRTEM micrographs recorded in the red boxes from (a) and (b), respectively.

as shown in Figure 2b. Similar to a-Mn_3O_4 ONCs composites, upon doping of c-Mn_3O_4 ONCs, fallen of V_{th} and V_{sat} were obtained, however, the maximum decreases of V_{th} and V_{sat} were just 16% and 13%, respectively. Figure 2c,d shows the trend of the T_{total} and C_{on} characteristics of a-Mn_3O_4 and c-Mn_3O_4 ONCs mixtures (The results list in the paper are the average values of at least three tests). The LCs composites had the coincidental lowest T_{total} and highest C_{on} values at 0.03 wt% doping concentration in the two systems. Compared with c-Mn_3O_4 composites which maximum C_{on} was 48, the C_{on} in a-Mn_3O_4 composites was remarkably enhanced and achieved to a drastic increase of 160%. Based on the systematic study on the driving voltage, contrast, and response time, it could be confirmed that the obviously enhanced E-O activities from a-Mn_3O_4 ONCs doping blends better than that from c-Mn_3O_4 ONCs doping blends. To the best of our knowledge, this was the first time such remarkable enhanced E-O activity of LCs has been observed from so trace of amorphous semiconductor nanomaterials doping. To further confirm the influence of crystallinity on E-O performance, the *V*–Tr curves for LC cells doped with different concentrations of amorphous-crystalline Mn_3O_4 ONCs were measured as shown in Figure S9 (Supporting Information). Similarly, the LCs composite with 0.03 wt% doping concentration had the lowest V_{th} and V_{sat} values (specific voltage in Table S3, Supporting Information), and we observed the following order on V_{th} and V_{sat}: amorphous Mn_3O_4 ONCs < amorphous-crystalline Mn_3O_4 ONCs < crystalline Mn_3O_4 ONCs. From all above results, we surmised that metastable electronic states in a-Mn_3O_4 ONCs easier escaped and transferred to LC molecular than that of c-Mn_3O_4 ONCs, in other words, the amorphous nanomaterials owned relatively high charge transfer occurring on the surface.[40,41]

In order to certify the effect of a-Mn_3O_4 ONCs on LCs, an organic replicating method was carried out. In this method,

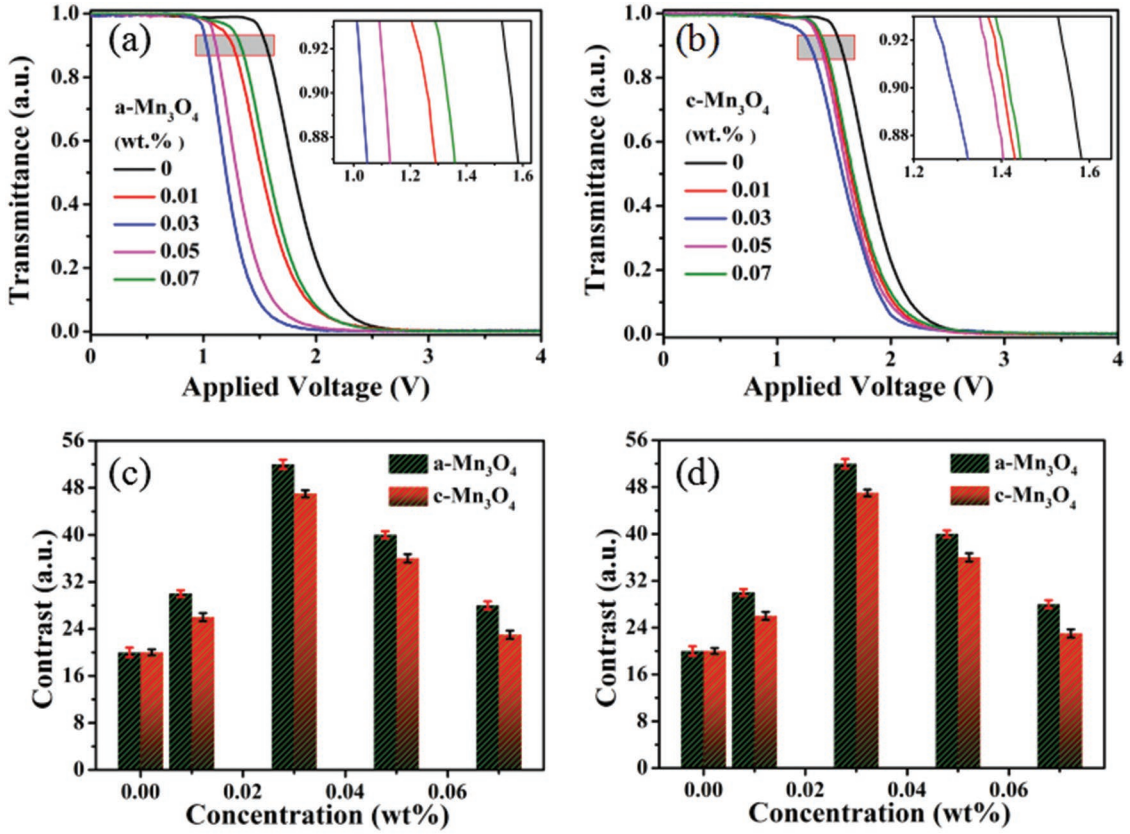

Figure 2. E-O properties of E7 and Mn_3O_4 ONCs composites. a),b) The V–Tr curves for LC cells doped with different concentrations of a- and c-Mn_3O_4 ONCs. c) The response time (T_{total}) and d) contrast (C_{on}) of E7 with various concentrations of a- and c-Mn_3O_4 ONCs doping. The concentrations varied from 0.01 wt% to 0.07 wt%. The illustrated error bars represent the variance of three measurements of three samples on the same concentration for each assay.

the distribution of a-Mn_3O_4 ONCs in the liquid crystal can be reflected intuitively. As shown in **Figure 3**, red oval circle places clearly shows that the polymer networks around a-Mn_3O_4 ONCs were biased towards the direction where there a-Mn_3O_4 ONCs, meaning that with a-Mn_3O_4 ONCs doping in E7 a perturbation generated in the LC matrix around the nanomaterials. We supposed that these perturbations were caused by charge transfer between nanocages and LCs. The charge transfer could change the liquid crystal dipole moment, then increasing the dielectric constant to reduce more threshold voltage.

Logically, a speculative mechanism was proposed to account for the enhanced E-O performance of the LCs in the presence of Mn_3O_4. **Figure 4**a showed the charges transformation processes from the c-Mn_3O_4 and a-Mn_3O_4 ONCs to LC molecules. Disordered long-range atomic arrangement and accommodating inherent abundant manganese defects confirmed by electron

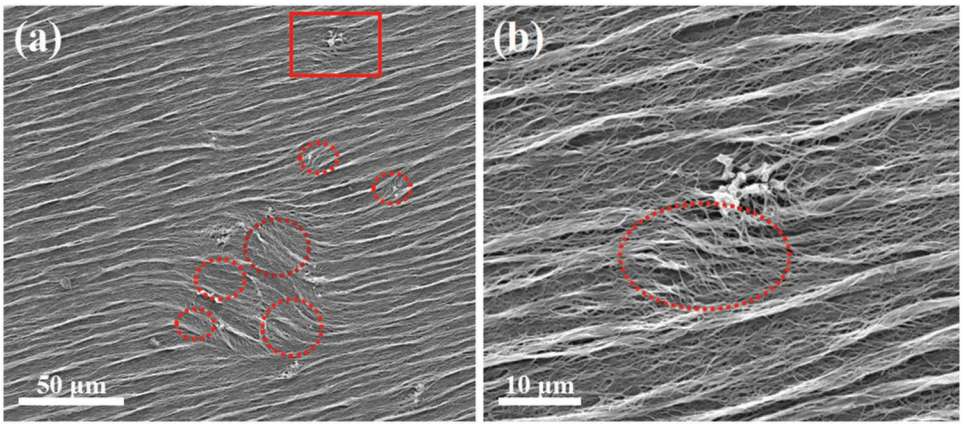

Figure 3. SEM of a-Mn_3O_4 ONCs in polymer network by organic replica, b) was a drawing enlarged red box from (a).

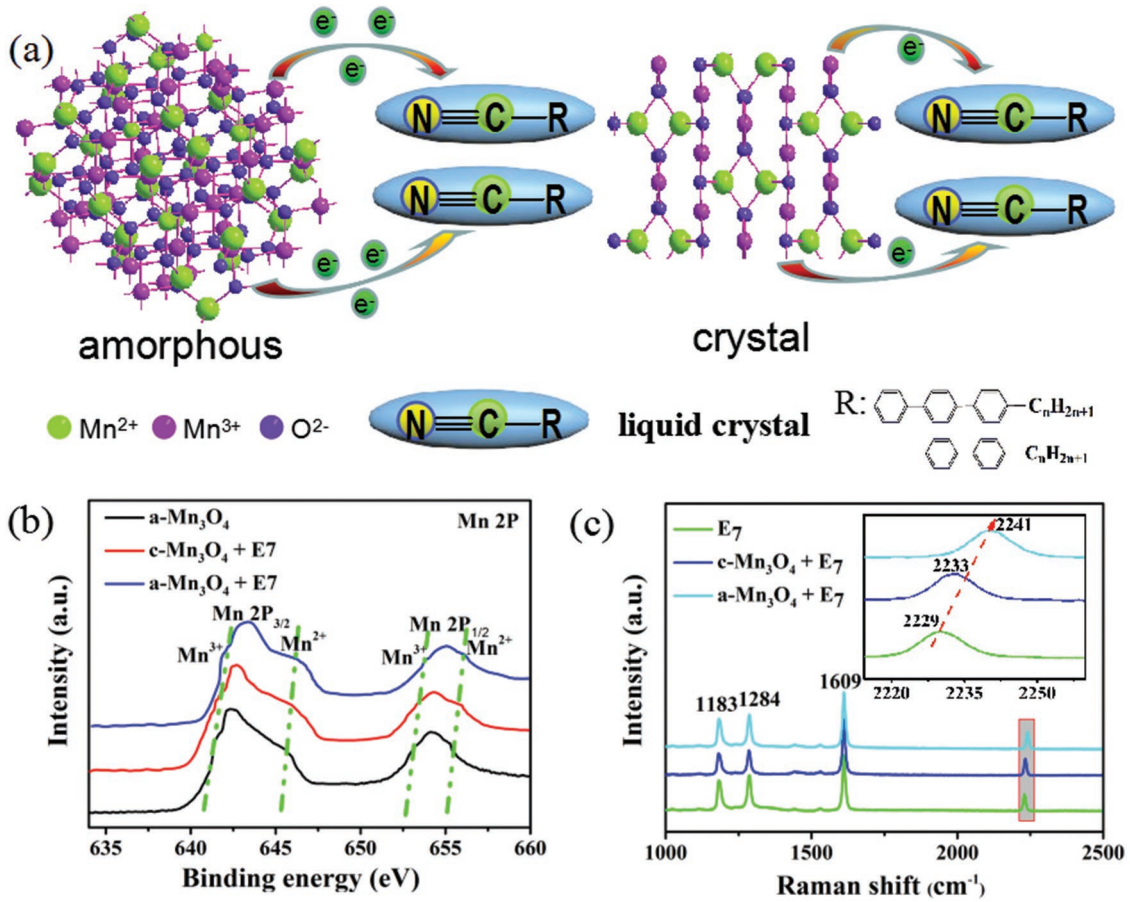

Figure 4. a) Concise schematic diagrams mechanism showing the charges transformation processes between the a-Mn_3O_4 and LC molecules. b) XPS spectra on Mn 2p of c- and a-Mn_3O_4 after blending with E7. c) Raman spectra of E7, c- and a-Mn_3O_4 and E7 blending.

spin resonance (ESR) spectra[42–44] (Figure S10, Supporting Information) endow a-Mn_3O_4 ONCs with dangling bonds and band tails, which could lead the energy to a metastable state and thus facilitate the surface electron escape and transfer. To verify interaction between the a-Mn_3O_4 and LC molecules in the system, XPS analyses and Raman measurements were performed. As displayed in the spectra of XPS on Mn 2p in Figure 4b, the a-Mn_3O_4 after composed with E7 exhibited higher intensity and larger peak-shift than that of c-Mn_3O_4 relative to raw a-Mn_3O_4 ONCs (the detail peaks positions were shown in Figure S11, Supporting Information). After mixed with E7, the peaks of Mn^{3+} (641.9 and 653.5 eV) shift to 642.3 and 654.1 eV, and Mn^{2+} (645.5 and 655.5 eV) shift to 645.9 and 656.3 eV. A similar effect was observed for the Raman spectra as shown in Figure 4c. After doping with Mn_3O_4, the signal of the cyano (−CN) vibration at 2229 cm^{-1} shifted to 2241 cm^{-1}, suggesting that the electric charges transfer from the a-Mn_3O_4 ONCs to the LC molecules. All these results strongly demonstrated that the intermolecular interaction in a-Mn_3O_4–LCs system was stronger than that of c-Mn_3O_4–LCs system, resulting from the differences in the electron-constraining ability of amorphous and crystalline nanomaterials.

The charges transferring from the substrate Mn_3O_4 ONCs to the LC molecules could increase the LC molecular electron density and redistribute the electron cloud, resulting in an obvious increase in the molecular dipole moment. As a result, the dielectric anisotropy of the liquid crystal further increased which would be propitious to the enhancement of E-O activity. Therefore, we probed the dielectric anisotropy of the a-Mn_3O_4 and c-Mn_3O_4–E7 composites as shown in **Figure 5**a. It is found that the dielectric anisotropy of a-Mn_3O_4–E7 composites was higher than that of c-Mn_3O_4–E7 composites. However, the threshold voltage for a twisted nematic (TN) LC cell not only depends on dielectric anisotropy but also the elastic constants of the LCs.[28] Therefore, we examined the elastic constants of the pure E7 and Mn_3O_4–E7 composites, as shown in Figure 5b,c (the numerical values were shown in Table S4, Supporting Information). By analyzing the experimental data, the twisting elastic constant (K_{22}) gradually decreased with the concentration of Mn_3O_4 ONCs increased from 0.01 to 0.03 wt% and started to increase when the concentration was greater than 0.03 wt%. We supposed that the decrease of K_{22} was related to the order parameter S of the LC molecules. The elastic constant was proportional to the square of the scalar order parameter S^2, a lower order parameter should lead to a decrease in elastic constants.[45] In the nanoparticles (NPs) and LCs composite system, the NPs could effectively dilute the LC mixture, thus leading to the decrease of the S.[28,46] Therefore, with addition of the Mn_3O_4 ONCs the K_{22} decreased in Mn_3O_4–E_7 composites and reached minimum value at the concentration of 0.03 wt%.

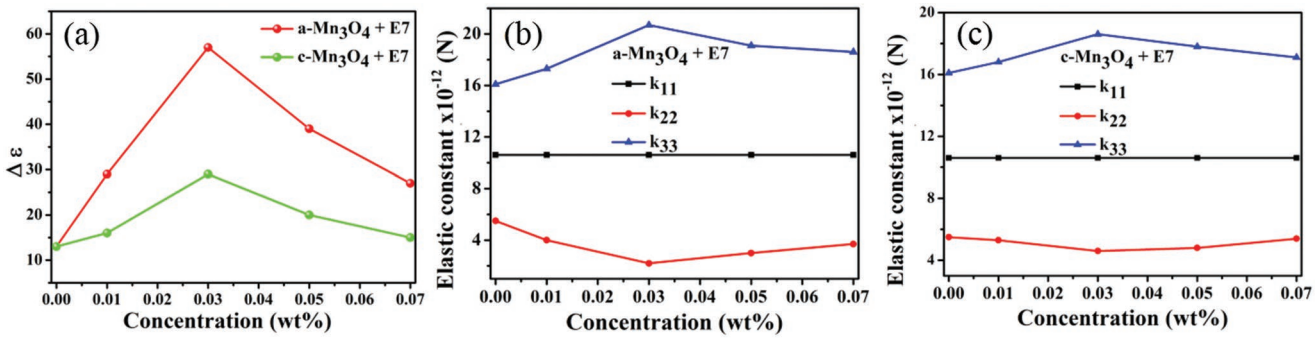

Figure 5. Variations of a) dielectric anisotropy, b,c) elastic constants with different Mn_3O_4 ONCs doping concentrations.

The change trend of the bending elastic constant (K_{33}) was opposite with K_{22}, and the K_{33} reached the maximum value at the concentration of 0.03 wt%. We supposed that the elastic energies of the Mn_3O_4-doped LCs increased under presence of Mn_3O_4 ONCs due to the strong anchoring between the LCs and the Mn_3O_4 ONCs, which was given expression to the K_{33}.[18,47] The splay elastic constant (K_{11}) remained unchanged under the presence of Mn_3O_4 ONCs. We speculated that phenomenon was due to the interaction between LC molecules and Mn_3O_4 ONCs which was not enough to influence the $K_{11,}$ since K_{11} was unfavorable in the liquid crystal as it requires greater energy than K_{33}.[48]

A concern for most NPs doped LC systems was the long-term stability. For investigating the stability of LCs doped with a-Mn_3O_4 ONCs, we controlled the same experimental environment as before and remeasured E-O performance, the comparison of data were shown in Figure S12 (Supporting Information). The curves of versus voltage were almost coincident with two independent measurements for at least one month (the specific V_{th} and V_{sat} were shown in Table S3, Supporting Information), and very slight variations were observed in the threshold and saturation voltages. For example, with the 0.03 wt% a-Mn_3O_4 doping concentration, the variation of V_{th} from 1.03 to 1.06 V and the change of V_{sat} from 1.54 to 1.59 V. In other words, the E7 doped with a-Mn_3O_4 ONCs exhibited long term stability of the E-O performance.

To investigate the reason that the concentration of a-Mn_3O_4 ONCs at 0.03 wt% doping LC cells exhibited the optimum E-O performance and exceeded 0.03 wt%, obtained the inferior E-O properties. Polarizing optical microscopy (POM) micrographs of LC cells doped with a-Mn_3O_4 ONCs were shown in Figure S13 (Supporting Information). The homogeneous dispersion of a-Mn_3O_4 ONCs in an LC host was observed in the doping concentration range of 0.01 to 0.03 wt%. When the concentration of a-Mn_3O_4 was greater than 0.03 wt%, aggregation of NPs in the LC host started to appear. As a result, the interaction between a-Mn_3O_4 ONCs and liquid crystals tended to be insufficient, so that charge transfer between a-Mn_3O_4 ONCs and LC molecules became faintly. The dielectric constant then decreased, which was consist with phenomenon in Figure 5a. The result confirmed that the dispersion of a-Mn_3O_4 ONCs in the LC host significantly affected the E-O properties of the nematic LCs.

In conclusion, we have demonstrated a facile strategy to synthesis a-Mn_3O_4 ONCs with shape-regularity and high uniformity, and successfully obtained the superior E-O performance blending with NLCs. As a result the maximum drop of V_{th} and V_{sat} was 34% and 31%, when the concentration of a-Mn_3O_4 ONCs was 0.03 wt%. The underlying mechanism behind this intriguing phenomenon was studied by using XPS analyses and Raman measurements, which showed that the intermolecular interaction in a-Mn_3O_4–LCs system was stronger than that of c-Mn_3O_4–LCs system. In addition to the remarkable E-O activity, the NLC E7 doped with a-Mn_3O_4 ONCs of different doping concentrations possessed long-term stability. Our general approach of blending inorganic amorphous semiconductor nanomaterials with liquid crystals might also meet subcomponent manufacturing standards and offer fabrication possibilities for devices with improved contrast ratios, faster switching speeds, and lower driving voltages.

Experimental Section

Materials: In this study, copper chloride ($CuCl_2$•$2H_2O$), potassium permanganate ($KMnO_4$), polyvinyl pyrrolidone (PVP) (average molecular weight: 30 000), ascorbic acid ($C_6H_8O_6$), phosphoric acid (H_3PO_4), and ethylene glycol (EG, 96%), ethanol (99.7%), and NaOH (96%) were from Beijing Chemical Works. A nematic liquid crystal (NLC), E7, was purchased from Shijiazhuang Cheng Zhi Yong Hua Display Material Co., Ltd. The polyvinyl alcohol (PVA) was from Alfa Aesar. All water used in experiments was deionized water. All reagents used in this experiment were of analytical grade without further purification.

Preparation of Cu_2O Octahedral Templates: The synthesis of Cu_2O templates based on our previous report.[38] $CuCl_2·2H_2O$ (0.17 g) was dissolved in deionized water (100 mL) at 55 °C, forming blue clarified solution. The polyvinyl pyrrolidone (4.5 g) was then added under stirring with 15 min. Then 2 M NaOH aqueous solution (10 mL) was added under stirring, and the solution gradually darkened. After 30 min stirring at the temperature of 55 °C, 0.6 M ascorbic acid aqueous solution (10 mL) was added drop wise into the mixture, yielding brick red precipitate. The mixture was stirred for 3 h at 55 °C. After cooling down, the precipitate was collected and washed with deionized water twice and ethanol three times by centrifugation to remove the residual inorganic ions and polymer, and finally dried under vacuum at 60 °C for 3 h for further characterization and use.

Synthesis of Amorphous Mn_3O_4 Octahedral Nanocages: In a typical synthesis, 5 mg Cu_2O octahedral nanocages and 7.5 mg $KMnO_4$ were dissolved in 40 mL deionized water to form a homogeneous mixed solution by ultrasonic vibration for 5 min. And then, 20 mL H_3PO_4 solution (0.02 mol L^{-1}) was slowly added to the mix solution through a constant pressure titration funnel maintained at 20 °C. After vigorous stirring for 2 h, the resulting precipitates were collected by centrifugation and decanting, washed with distilled water and absolute ethanol several times, and dried under vacuum at 60 °C for 5 h for

further characterization and use. The products were amorphous Mn_3O_4 Octahedral nanocages.

Synthesis of Crystalline Mn_3O_4 Octahedral Nanocages: Crystalline Mn_3O_4 ONCs were prepared by heat treatment of amorphous Mn_3O_4 ONCs at 400 °C for 2 h in Ar air.

Preparation of LC/Mn_3O_4 Octahedral Nanocages Composite: The Mn_3O_4 octahedral nanocages dispersed in *n*-hexane solvent were injected into E7 to prepare the mixed solution with different concentrations. The mixed solution was placed one day at room temperature to remove the *n*-hexane solvent, then using ultrasonic irradiation for an hour to promote Mn_3O_4 ONCs to disperse into E7 evenly. Finally, the composites of Mn_3O_4 ONCs at mass fractions of 0, 0.01, 0.03, 0.05, and 0.07 wt% were obtained.

Liquid Crystal Samples Cell Fabrication: The TN LC cells were made using 2.0 cm × 3.0 cm glass substrates coated with the indium tin oxide (ITO). The glass plates were coated with PVA using a spin coater. These coated substrates were prebaked at 80 °C for 30 min in an oven. The baked, PVA-coated substrates were rubbed with velvet to get uniform grooves on PVA. Then, the TN cells were prepared with a cell gap of about 8 µm to measure the E-O characteristics. The N-LC mixtures were injected into the each cell by capillary action at room temperature, respectively.

Electro-Optic (E-O) Properties Measurements: E-O properties were measured using the LCT-5066C LCD (North LCD Engineering Research and Development Center, China) integrated parametric tester. The E-O properties of E7 doped with Mn_3O_4 were investigated. V_{th} and V_{sat} are defined as the driving voltages when the light transmittance was 90% and 10% in the on-stage, respectively. C_{on} refers to the ratio of the maximum light transmittance to the minimum light transmittance. Response time (T_{total}) includes T_{on} and T_{off}, T_{on} and T_{off} are the response time when the light transmittance changed from 90% to 10% in the on-stage and from 10% to 90% in the off-stage, respectively.

Dielectric Anisotropy Measurements: The dielectric anisotropy parameters of the prepared samples were calculated from electric capacity measured by WK Kerr Electronics 6500B analyzer at the frequency of 1 KHz. The bridge applied a direct current bias voltage of 0–20 V to the cell electrodes, which reoriented the liquid crystals inside the cell allowing the extraction of C_0 and C_∞ from a single measurement, then the $\varepsilon_{\parallel}$ and $\varepsilon_{\perp}$ were calculated. The dielectric anisotropy for the liquid crystals could be expressed by the following relation

$$\Delta\varepsilon = \varepsilon_{\parallel} - \varepsilon_{\perp}$$

where $\varepsilon_{\parallel}$ was the dielectric constant in the direction parallel to the director and $\varepsilon_{\perp}$ was the dielectric constant in perpendicular to the director.

Elastic Constants Measurements: The splay elastic constant and bend elastic constant of the prepared samples were extracted from ALCT-PP1equipment by capacitance–voltage (CV) measurement. The pure LC E7 and Mn_3O_4 ONCs composites were filled in antiparallel rubbed LC cells, the ALCT accurately measured samples capacitance as a function of applied voltage and fit the measured data generated from the fitted model using the calculated physical properties which were then available to the ALCT user (gold). The closer fitting to the experiment, the more precise electrical measurements and more accurate model. Then the splay elastic constant and the bend elastic constant were derived. The twist elastic constant of the samples was extracted from ALCT-K_{22}-1equipment. The pure LC E7 and Mn_3O_4 ONCs composites filled in antiparallel rubbed LC cells, so that with no applied electric field minimum light was transmitted. A high electric field was applied to the cell to drive the cell to a maximum light transmittance state, after which the electrical field was removed. The transmittance as a function of time $T(t)$, decreases and was measured as the liquid crystal was allowed to relax, and the transmittance curve was processed to give a time-dependent azimuth angle, then the twist elastic constant was calculated.

SEM Measurements for Organic Replica: The samples were prepared as follows. First, the LC of E7 mixed with a-Mn_3O_4 NCs, the photoinitiator (651), and the photopolymerizable monomer (C6M) was filled in the TN cell. Under UV irradiation with 18 mW cm^{-2} for 1 h, then the cell was immersed in cyclohexane about 2 d to remove LCs. Next, the cells were opened cautiously to get glass substrates. Finally, the substrate with polymer network and a-Mn_3O_4 NCs were coated with a thin layer of platinum for SEM observation.

Supporting Information

Supporting Information is available from the Wiley Online Library or from the author.

Acknowledgements

G.M. and B.J. contributed equally to this work. The authors acknowledge the financial support of the National Natural Science Foundation of China (51532001 and 51673008) and the National Key R&D Program of China (2018YFB0703703).

Conflict of Interest

The authors declare no conflict of interest.

Keywords

amorphous Mn_3O_4, charge transfer, electro-optic properties, liquid crystals

Received: December 21, 2018
Revised: March 25, 2019
Published online: April 12, 2019

[1] S. Aya, H. Obara, D. Pociecha, F. Araoka, K. Okano, K. Ishikawa, E. Gorecka, T. Yamashita, H. Takezoe, *Adv. Mater.* **2014**, *26*, 1918.
[2] V. Borshch, S. V. Shiyanovskii, O. D. Lavrentovich, *Phys. Rev. Lett.* **2013**, *111*, 107802.
[3] O. Buchnev, N. Podoliak, T. Frank, M. Kaczmarek, L. Jiang, V. A. Fedotov, *ACS Nano* **2016**, *10*, 11519.
[4] C. Lapointe, A. Hultgren, D. M. Silevitch, E. J. Felton, D. H. Reich, R. L. Leheny, *Science* **2004**, *303*, 652.
[5] Y. Y. Luk, N. L. Abbott, *Science* **2003**, *301*, 623.
[6] M. Mitov, C. Portet, C. Bourgerette, E. Snoeck, M. Verelst, *Nat. Mater.* **2002**, *1*, 229.
[7] T. Z. Shen, S. H. Hong, J. K. Song, *Nat. Mater.* **2014**, *13*, 394.
[8] Y. Xia, T. S. Mathis, M. Q. Zhao, B. Anasori, A. Dang, Z. Zhou, H. Cho, Y. Gogotsi, S. Yang, *Nature* **2018**, *557*, 409.
[9] A. Sawada, K. Tarumi, S.-H. Naemura, *Jpn. J. Appl. Phys.* **1999**, *38*, 1418.
[10] S. P. Yadav, M. Pande, R. Manohar, S. Singh, *J. Mol. Liq.* **2015**, *208*, 34.
[11] O. Yaroshchuk, S. Tomylko, O. Kovalchuk, N. Lebovka, *Carbon* **2014**, *68*, 389.
[12] H. Yoshida, K. Kawamoto, H. Kubo, T. Tsuda, A. Fujii, S. Kuwabata, M. Ozaki, *Adv. Mater.* **2010**, *22*, 622.
[13] M. Prévôt, M. Amela-Cortes, S. K. Manna, R. Lefort, S. Cordier, H. Folliot, L. Dupont, Y. Molard, *Adv. Funct. Mater.* **2015**, *25*, 4966.
[14] G. Singh, M. Fisch, S. Kumar, *Rep. Prog. Phys.* **2016**, *79*, 056502.
[15] A. Mertelj, D. Lisjak, M. Drofenik, M. Copic, *Nature* **2013**, *504*, 237.
[16] M. Yakemseva, I. Dierking, N. Kapernaum, N. Usoltseva, F. Giesselmann, *Eur. Phys. J. E* **2014**, *37*, 7.

[17] Y. Zhang, Q. K. Liu, H. Mundoor, Y. Yuan, I. I. Smalyukh, *ACS Nano* **2015**, *9*, 3097.
[18] A. Chandran, J. Prakash, K. K. Naik, A. K. Srivastava, R. Dąbrowski, M. Czerwiński, A. M. Biradar, *J. Mater. Chem. C* **2014**, *2*, 1844.
[19] S. K. Prasad, M. V. Kumar, C. V. Yelamaggad, *Carbon* **2013**, *59*, 512.
[20] W. K. Lee, S. J. Hwang, M.-J. Cho, H. G. Park, J. W. Han, S. J. Song, J. H. Jang, D. S. Seo, *Nanoscale* **2013**, *5*, 193.
[21] W. K. Lee, Y. S. Choi, Y. G. Kang, J. Sung, D. S. Seo, C. Park, *Adv. Funct. Mater.* **2011**, *21*, 3843.
[22] D. Y. Zhao, L. H. Xu, Y. Shang, X. X. Li, L. Guo, *Nano Res.* **2018**, *11*, 4836.
[23] B. Liu, Y. Ma, D. Y. Zhao, L. H. Xu, F. S. Liu, W. Zhou, L. Guo, *Nano Res.* **2017**, *10*, 618.
[24] B. Kinkead, T. Hegmann, *J. Mater. Chem.* **2010**, *20*, 448.
[25] S. Acharya, S. Kundu, J.-P. Hill, G.-J. Richards, K. Ariga, *Adv. Mater.* **2009**, *21*, 989.
[26] Y. Reznikov, O. Buchnev, O. Tereshchenko, *Appl. Phys. Lett.* **2003**, *82*, 1917.
[27] M. Kaczmarek, O. Buchnev, I. Nandhakumar, *Appl. Phys. Lett.* **2008**, *92*, 103307.
[28] N. Podoliak, O. Buchnev, M. Herrington, E. Mavrona, M. Kaczmarek, A. G. Kanaras, E. Stratakis, J. F. Blach, J. F. Henninot, M. Warenghem, *RSC Adv.* **2014**, *4*, 46068.
[29] Z. H. Stachurski, *Materials* **2011**, *4*, 1564.
[30] Y. A. Shu, B. S. Fales, B. G. Levine, *Nano Lett.* **2015**, *15*, 6247.
[31] Z. Y. Wang, Z. C. Wang, W. T. Liu, W. Xiao, X. W. Lou, *Energy Environ. Sci.* **2013**, *6*, 87.
[32] J. Z. Liu, Y. F. Ji, J. W. Nai, X. G. Niu, Y. Luo, L. Guo, S. H. Yang, *Energy Environ. Sci.* **2018**, *11*, 1736.
[33] P. A. Khomyakov, W. Andreoni, N. D. Afify, A. Curioni, *Phys. Rev. Lett.* **2011**, *107*, 255502.
[34] J. X. Feng, S. H. Ye, X. F. Lu, Y. X. Tong, G. R. Li, *ACS Appl. Mater. Interfaces* **2015**, *7*, 11444.
[35] T. T. Li, B. Xue, B. W. Wang, G. N. Guo, D. D. Han, Y. C. Yan, A. G. Dong, *J. Am. Chem. Soc.* **2017**, *139*, 12133.
[36] R. Rahimi, A. Mehrehjedy, S. Zargari, *Environ. Prog. Sustainable Energy* **2017**, *36*, 1439.
[37] S. L. Yin, X. M. Wang, Z. G. Mou, Y. J. Wu, H. Huang, M. S. Zhu, Y. K. Du, P. Yang, *Phys. Chem. Chem. Phys.* **2014**, *16*, 11289.
[38] D. F. Zhang, H. Zhang, L. Guo, K. Zheng, X. D. Han, Z. Zhang, *J. Mater. Chem.* **2009**, *19*, 5220.
[39] D. P. Dubal, A. D. Jagadale, C. D. Lokhande, *Electrochim. Acta* **2012**, *80*, 160.
[40] X. T. Wang, W. X. Shi, Z. Jin, W. F. Huang, J. Lin, G. S. Ma, S. Z. Li, L. Guo, *Angew. Chem., Int. Ed.* **2017**, *56*, 9851.
[41] J. Z. Liu, J. W. Nai, T. T. You, P. F. An, J. Zhang, G. S. Ma, X. G. Niu, C. Y. Liang, S. H. Yang, L. Guo, *Small* **2018**, *14*, 1703514.
[42] A. V. Jagannadham, P. Venkateswarlu, *Proc. Indian Acad. Sci., Sect. A* **1971**, *74*, 34.
[43] R. J. Richardson, S. Lee, T. J. Menne, *Phys. Rev. B* **1971**, *4*, 3837.
[44] V. P. Shrivastava, P. Venkateswarlu, *Proc. Indian Acad. Sci., Sect. A* **1966**, *63*, 284.
[45] L. M. Blinov, V. G. Chigrinov, *Electro-Optic Effects in Liquid Crystal Materials*, Springer-Verlag, New York **1994**.
[46] I. Abdulhalim, *J. Nanophotonics* **2012**, *6*, 061001.
[47] S. Y. Jeon, S. H. Shin, S. J. Jeong, S. H. Lee, S. H. Jeong, Y. H. Lee, H. C. Choi, K. J. Kim, *Appl. Phys. Lett.* **2007**, *90*, 121901.
[48] W. Wang, T. Hashimoto, G. Lieser, G. Wenger, *J. Polym. Sci., Part B: Polym. Phys.* **1994**, *32*, 2171.